Optimizing Ohmic contacts to Nd-doped ntype SrSnO₃

Cite as: Appl. Phys. Lett. **118**, 142104 (2021); https://doi.org/10.1063/5.0027470 Submitted: 28 August 2020 . Accepted: 07 March 2021 . Published Online: 07 April 2021

DV. R. Saran Kumar Chaganti, Prafful Golani, Tristan K. Truttmann, Fengdeng Liu, Bharat Jalan, and Steven J. Koester

COLLECTIONS

Paper published as part of the special topic on Ultrawide Bandgap Semiconductors







ARTICLES YOU MAY BE INTERESTED IN

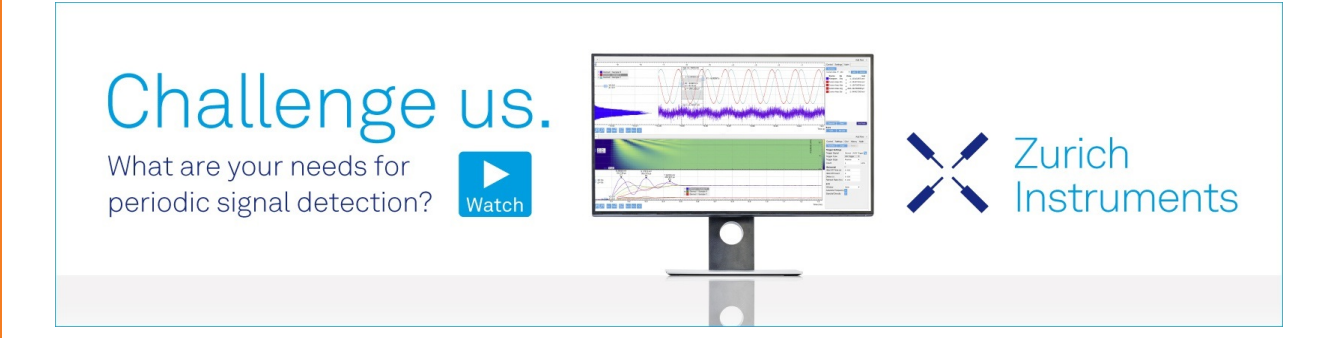
Half-Heusler thermoelectric materials

Applied Physics Letters 118, 140503 (2021); https://doi.org/10.1063/5.0043552

Highly efficient and stable electroluminescence from Er-doped Ga₂O₃ nanofilms fabricated by atomic layer deposition on silicon

Applied Physics Letters 118, 141104 (2021); https://doi.org/10.1063/5.0049556

Prospects for application of ferroelectric manganites with controlled vortex density Applied Physics Letters 118, 140502 (2021); https://doi.org/10.1063/5.0032988





Optimizing Ohmic contacts to Nd-doped n-type SrSnO₃

Cite as: Appl. Phys. Lett. **118**, 142104 (2021); doi: 10.1063/5.0027470 Submitted: 28 August 2020 · Accepted: 7 March 2021 · Published Online: 7 April 2021







V. R. Saran Kumar Chaganti,¹ 🍺 Prafful Golani,¹ 皟 Tristan K. Truttmann,² 🕞 Fengdeng Liu,^{1,2} Bharat Jalan,² 皟 and Steven J. Koester^{1,a)} 📵

AFFILIATIONS

 1 Department of Electrical and Computer Engineering, University of Minnesota, Minneapolis, Minnesota 55455, USA

Note: This paper is part of the Special Topic on Ultrawide Bandgap Semiconductors.

ABSTRACT

We report the results of metal contact resistance, $R_{\rm C}$, to Nd-doped n-type SrSnO $_3$ films grown by radical-based hybrid molecular beam epitaxy. Sc, Mn, Ti, Al, and Cr contact layers were deposited onto heavily doped SrSnO $_3$ thin films. With no annealing, Al and Cr contacts were found to be highly resistive, while Sc, Mn, and Ti were more conductive, with Mn having the lowest $R_{\rm C}$ of $11 \pm 3~\Omega$ -mm, immediately after liftoff. After Al $_2$ O $_3$ passivation at 200 °C, Sc, Mn, and Ti contacts all showed Ohmic behavior, with Ti contacts having $R_{\rm C} = 2.4 \pm 0.3~\Omega$ -mm and a resultant sheet resistance, $R_{\rm S}$, of $1.66 \pm 0.07~{\rm k}\Omega/{\rm m}$. Specific contact resistivity, $\rho_{\rm C}$, values of 0.03, 0.2, and 0.5 m Ω -cm 2 were determined for Ti, Sc, and Mn, respectively. Annealing at 300 °C did not result in any significant change in $R_{\rm C}$. An additional study was performed using Ti-contacts on bi-layer films consisting of a heavily doped cap layer grown on a moderately doped active layer. It was found that the $R_{\rm C}$ ($\rho_{\rm C}$) of Ti metal to the bi-layer films was \sim 1 (2) order(s) of magnitude lower than on single-layer controls. Temperature-dependent analysis was used to extract the barrier height and doping effect for annealed Ti contacts. This work is an important step in evaluating SrSnO $_3$ for use in high-performance and transparent electronic applications.

Published under license by AIP Publishing. https://doi.org/10.1063/5.0027470

Ultra-wide gap (UWG) semiconductors with the bandgap, E_G , in the range of 4-6 eV can offer significant device performance improvements over their narrow-gap counterparts in high-power electronics and provide new opportunities for use in deep-UV optoelectronics and extreme-environment applications. Perovskite stannates, including BaSnO₃, SrSnO₃, and CaSnO₃, are emerging wide gap semiconductors that are capable of high mobilities at unusually high carrier concentrations owing to their relatively high dielectric constant, low phonon scattering, and light electron effective mass.^{2–4} SrSnO₃ (SSO), which has an E_G in the range of 4–5 eV (Refs. 5–8), could offer particular advantages over other UWG semiconductors including a wide range of heterostructure opportunities that can provide band offsets > 2 eV and potential for integration with other functional perovskites.^{2,8} High-quality epitaxial SSO films have been grown using radical-based hybrid molecular-beam epitaxy (MBE),9-11 effect transistors (FETs) with promising performance have recently been demonstrated. 12-14 Early reports on SSO MESFETs with Sc contacts showed high contact resistance, $R_{\rm C}$, ¹² and while improved contacts to SSO using Ti metallization were recently reported, 13 a comprehensive study of contacts to SSO has not been performed.

Here, we report a systematic study of metallization and annealing on the performance of contacts to heavily doped SSO. We attempt to exploit one of the key features of SSO that this material can achieve very high doping levels above $10^{20}\,\mathrm{cm}^{-3}$ while still maintaining relatively high carrier mobility. These properties can be exploited to produce low $R_{\rm C}$, particularly if combined with the use of a low-work function metal to produce tunneling band edge contacts. The low effective mass in SSO of $\sim\!0.3-0.4~m_0$ further allows for high tunneling probabilities and thus lower $R_{\rm C}$. Here, we report the results of contact work function engineering on Nd-doped n-type SSO thin films. We found that Ti contacts had the lowest $R_{\rm C}$ and specific contact resistivity, $\rho_{\rm C}$, after annealing, with values as low as 2.4 Ω -mm and 0.03 m Ω -cm², respectively. To demonstrate the dependence of $R_{\rm C}$ and $\rho_{\rm C}$ on doping, results of Ti contacts on bi-layer films with a heavily doped cap layer are also reported.

Using a procedure similar to that described in Refs. 9-11 and 15, all films used were grown by radical-based hybrid MBE on insulating $GdScO_3$ (GSO) substrates. Sn is supplied via a chemical precursor hexamethylditin (HMDT) whose volatility and high reactivity help to achieve an adsorption-controlled growth regime and stoichiometric

²Department of Chemical Engineering and Materials Science, University of Minnesota, Minneapolis, Minnesota 55455 USA

^{a)}Author to whom correspondence should be addressed: skoester@umn.edu

SSO films. Nd was utilized as the *n*-type dopant and was supplied using an effusion cell for all the films. The details of the growth beyond the summary provided here can be found elsewhere.9 One set of films utilized here consisted of a 10-nm-thick undoped SSO buffer layer, followed by a 26-nm-thick Nd-doped SSO active layer. The doping was controlled by setting the Nd effusion cell temperature, $T_{\rm Nd}$, to 940 °C. Van der Pauw measurements performed on the as-grown films yielded a high carrier concentration of $3.5 \times 10^{19} \, \text{cm}^{-3}$, a roomtemperature Hall mobility, $\mu = 37 \text{ cm}^2/\text{V}$ s, and a sheet resistance, $R_{\rm S} = 1874 \ \Omega/\Box$, at room temperature. From here on, this film will be referred to as "SSO_Heavy" [Fig. 1(a)]. The bi-layer sample used in the additional contact experiment consisted of a 10-nm-thick undoped SSO buffer layer, a 26-nm-thick Nd-doped SSO layer grown using $T_{\rm Nd}$ = 915 °C, and a 9-nm-thick Nd-doped SSO cap layer grown with the $T_{\rm Nd}$ = 950 °C. The single-layer film, used as a control sample, was grown using the exact same conditions as in the bi-layer sample but was grown without the heavily doped cap layer. The single- and bilayer films will be referred to as "SSO_Control" [Fig. 1(b)] and "SSO_Bilayer" [Fig. 1(c)], respectively. While the as-grown properties of SSO_Bilayer were not independently measured, SSO_Control was found to have a carrier concentration of $2.3 \times 10^{19} \, \text{cm}^{-3}$, $\mu = 28 \, \text{cm}^2$ / V s, and $R_S = 3845 \ \Omega/\Box$. The films were characterized by highresolution x-ray diffraction (HR-XRD) and the results are summarized in Figs. 1(d)-1(f). The coupled scans show an out-of-plane pseudocubic lattice parameter of $a_{pc} = 4.110 \pm 0.006 \,\text{Å}$, consistent with a mostly coherent film with the strain-stabilized tetragonal phase of SrSnO₃. A small shoulder at higher 2θ represents a small volume fraction of the room-temperature orthorhombic phase.

In order to measure $R_{\rm C}$, transfer-length method (TLM) structures were fabricated on the SSO_Heavy sample and measured. The detailed fabrication sequence is provided in the supporting material. The TLMs utilized standard mesa isolation defined using reactive ion etching (RIE). Various different metals with low work function, $\Phi_{\rm M}$, were analyzed including Sc ($\Phi_{\rm M} = 3.7~{\rm eV}$), Mn ($\Phi_{\rm M} = 4.1~{\rm eV}$), and Ti ($\Phi_{\rm M} = 4.3~{\rm eV}$). For the TLMs fabricated on the SSO_Bilayer and SSO_Control samples, the fabrication procedure was similar, except that after SSO_Bilayer mesa formation, a recess etch using RIE was performed in order to partially remove the heavily doped cap layer. On the SSO_Bilayer and SSO_Control samples, only TLMs with Ti contacts were studied.

The annealing sequence was also different for the two sample sets. For SSO_Heavy, after contact formation, the samples were immediately passivated using atomic layer deposition (ALD) of Al $_2$ O $_3$ at 200 °C. After electrical characterization, a subsequent 300 °C anneal was also performed. For SSO_Bilayer and SSO_Control, after contact metallization, the samples were annealed at successively increasing temperatures, up to 300 °C in forming gas. After these annealing steps, ALD passivation with Al $_2$ O $_3$ at 200 °C was performed. Figures 1(g)–1(i) show cross-sectional schematics of the final TLM structures for all three epi-layer samples after fabrication.

Figure 2(a) shows an optical micrograph of the TLM structures fabricated on the SSO_Heavy film. The current vs voltage curves obtained from the TLM structures based on Ti-, Mn-, and Sc-contacts are shown in Figs. 2(b), 2(c), and 2(d), respectively. All three contact metals show Ohmic behavior. These measurements were obtained after ALD Al_2O_3 deposition, which was an \sim 1 h long process while

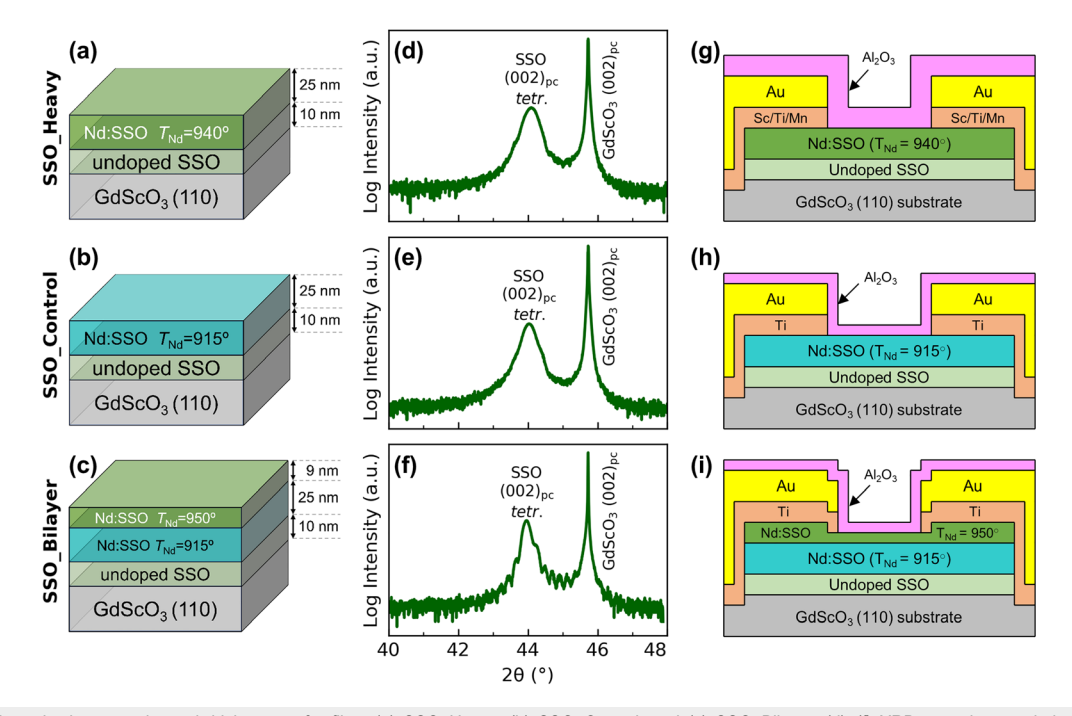


FIG. 1. (a)–(c) show the layer stacks and thicknesses for films (a) SSO_Heavy, (b) SSO_Control, and (c) SSO_Bilayer. (d)–(f) XRD specular coupled scans for films (d) SSO_Heavy, (e) SSO_Control, and (f) SSO_Bilayer. (g)–(i) Schematics showing the layers after fabrication of the TLM structures for (g) SSO_Heavy, (h) SSO_Control, and (i) SSO_Bilayer. Sc, Mn, or Ti contacts were used on SSO_Heavy, whereas only Ti contacts were used on the other two films. The temperatures indicated in the plots represent the Nd effusion cell temperature during growth in units of °C.

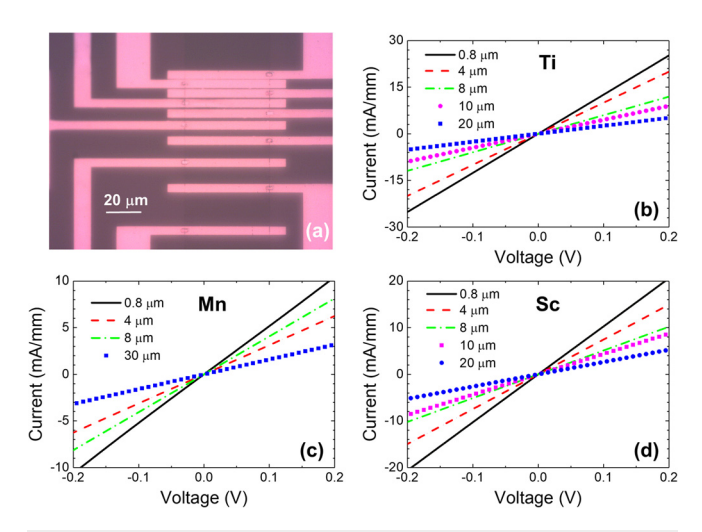


FIG. 2. (a) Optical micrograph of the TLM structure fabricated on SSO_Heavy sample with a contact finger width of 5 μ m. (b)–(d) Current vs voltage curves obtained from TLM structures for Ti, Mn, and Sc metal contacts, respectively. The curves corresponding to (b) Ti contacts, (c) Mn contacts, and (d) Sc contacts, after ALD passivation at 200 °C.

the substrate was continuously heated at 200 °C. Thus, the ALD deposition can be considered as an annealing process, as well as a passivation step. Ohmic contacts based on Cr and Al were also explored in separate experiments and were found to be highly resistive when measured at room temperature without any passivation (Fig. S1). Based on prior results, 12 the Sc contacts are not expected to show Ohmic behavior when measured at room temperature before any annealing. Other experiments showed that Ti contacts also tend to produce high and variable resistances when measured before annealing (Fig. S2). These results support the hypothesis that the ALD step not only passivates but also anneals the contacts.

To extract the $R_{\rm C}$ values and transfer lengths, $L_{\rm T}$, width-normalized resistances were determined from current-voltage measurements performed for different contact spacings. This procedure was performed immediately after metal liftoff, after the 200 °C Al₂O₃ passivation step, and finally, after the subsequent 300 °C forming gas anneal. Initially, after liftoff, only the Mn-contacted sample had linear contacts (which had $R_{\rm C}=11\pm3~\Omega$ -mm), while Ti and Sc produced very high-resistance, non-linear contacts. After the 200 °C Al₂O₃ deposition, however, all three metals produced Ohmic contacts, which allowed extraction of the contact resistance. The results after the 200 °C ALD deposition and after subsequent 300 °C annealing are shown in Figs. 3(a) and 3(b), respectively.

The corresponding $R_{\rm C}$, $R_{\rm S}$, $L_{\rm T}$, and $\rho_{\rm C}$ values extracted from the data in Fig. 3 for all three metals are summarized in Table S1. The $R_{\rm S}$ values are lower than, but close to, those obtained from as-grown film values based upon van der Pauw measurements. The small reduction in $R_{\rm S}$ could be due to passivation of surface states by the Al₂O₃, which would make more carriers available in the channel. The Ti contacts providing the lowest $R_{\rm C}$ as well as the least variability and subsequent annealing at 300 °C did not provide substantial improvement. The minimum $R_{\rm C}$ obtained for Ti contacts is a \sim 15× improvement over the previous value obtained using Sc contacts, ¹² while the Sc contacts

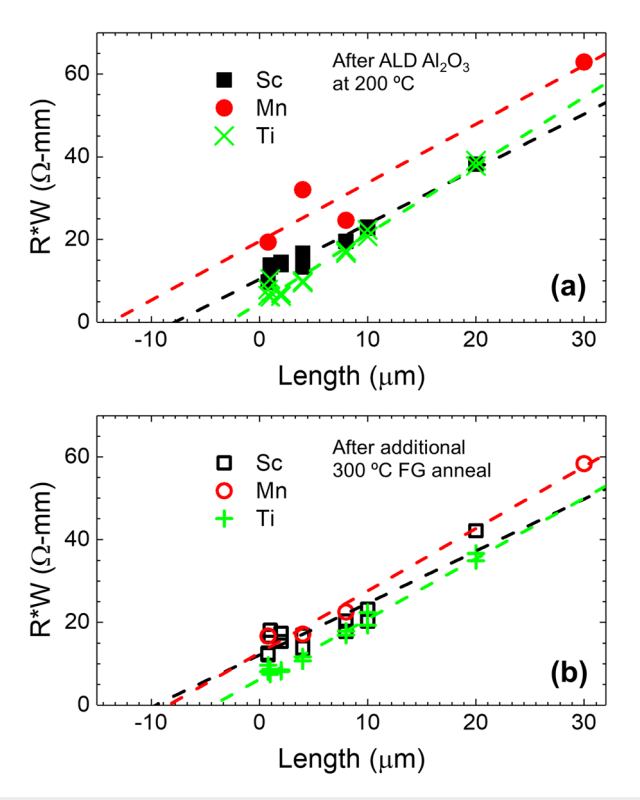


FIG. 3. Contact resistance extraction for Sc-, Mn-, and Ti-contacts on SSO_Heavy samples after (a) ALD passivation at 200 $^{\circ}$ C and (b) and additional 300 $^{\circ}$ C forming gas anneal.

used in this work registered a \sim 5× improvement compared to Ref. 12, which we attribute to the reduced atmospheric degradation as a result of the protective passivation layer. The Ti contacts with $R_{\rm C}=2.4\pm0.3$ Ω -mm also displayed the lowest extrapolation error, suggesting that Ti produces the most consistent contacts of the metals evaluated. Additional studies are needed to understand the reasons for the superior performance of the Ti metallization. The value of $\rho_{\rm C}$ was calculated for the three metals using the $L_{\rm T}$ values obtained from the x-intercepts in Fig. 3. The smaller $L_{\rm T}$ of 1.4 μ m obtained for the Ticontacts indicates that these contacts are far superior in comparison to the Sc- and Mn-contacts. (For the Mn-contacts, because the extracted transfer length was greater than the contact width itself, the contact width of 5 μ m was used for the $\rho_{\rm C}$ extraction.) $\rho_{\rm C}$ values as low as 34 \pm 6 $\mu\Omega$ -cm² were obtained for Ti-contacts, which is \sim 14× and \sim 5× improvement over Mn- and Sc-contacts, respectively.

In order to evaluate the effect of doping on $R_{\rm C}$, Ti-contacts on SSO_Bilayer and SSO_Control films were compared. As explained earlier, the SSO_Control film does not have a heavily doped cap layer, while the SSO_Bilayer film has a heavily doped cap layer on top of an active layer with the same doping as in SSO_Control. For the SSO_Control and SSO_Bilayer films, annealing up to 300 °C was performed without passivation and then both the films were passivated with ALD Al₂O₃. The ALD passivation was performed after the 300 °C annealing step because the Ti-contacts showed less degradation in atmosphere compared to the Sc contacts based on our prior experience. A comparison of the TLM data obtained on the two films after

300 °C annealing and after the subsequent ALD passivation is shown in Fig. 4. Clearly, the SSO_Bilayer sample provides much lower resistance at each spacing length. The extracted $R_{\rm C}$, $R_{\rm S}$, $\rho_{\rm C}$, and $L_{\rm T}$ values obtained on the two films are summarized in Table S2. The error bars for the data obtained on SSO_Bilayer are high partly because the actual $R_{\rm C}$ values are very small. Despite the error bar, the improvement offered by the bi-layer structure is obvious from Fig. 4 and the data in Table S2. The low $\rho_{\rm C}$ values are promising for the use of heavily doped SSO for future transistor applications.

The dependence of contact resistance on annealing temperature (prior to passivation) for the Ti contacts on SSO_Control and SSO_Bilayer was also studied (Fig. S3). The contacts on both samples were found to be highly resistive after 150 °C annealing. The contacts on the SSO_Films transitioned to low resistance after 225 °C annealing, while the SSO_Bilayer films improved only after the 300 °C anneal. We suspect that an insulating barrier at the metal/SSO interface could be the reason for the much higher contact resistivity before annealing, ¹¹ though further studies are needed to understand the precise nature of the metal–SSO interface.

Finally, to evaluate whether the extracted specific contact resistivities agree with expectations, we have performed temperature-dependent TLM experiments combined with theoretical modeling. Full details are provided in the Supporting Information. The extracted $\rho_{\rm C}$ vs T results are summarized in Table S3 for both SSO_Bilayer and SSO_Control. The contact resistance for SSO_Bilayer remains within the noise floor down to 77 K. However, for SSO_Control, both $R_{\rm C}$ and

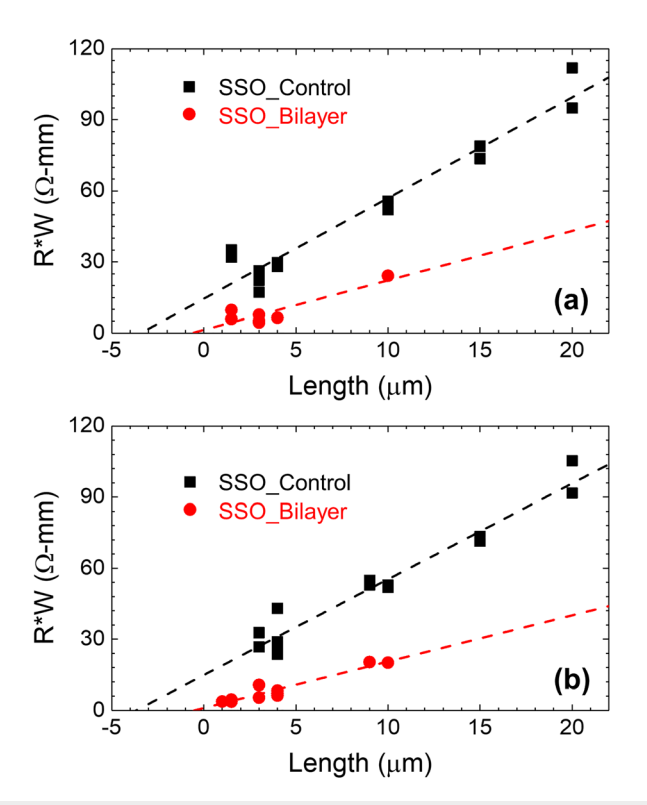


FIG. 4. Contact resistance extraction for Ti-contacts on SSO_Bilayer and SSO_Control samples obtained after (a) $300\,^{\circ}$ C anneal and (b) subsequent ALD passivation.

 $\rho_{\rm C}$ increase weakly with decreasing temperature, suggesting a process primarily dominated by field emission (FE), though with some degree of thermally activated transport.

In order to better quantify the Schottky barrier properties for SSO_Control, we modeled the contacts to the single-layer films using standard Schottky barrier theory. ¹⁶ Here, the electron current density, *J*, was obtained from

$$J = \frac{A^*T}{k} \int_{E_{CS}}^{\infty} T(E) \frac{\ln(1 + f_S)}{\ln(1 + f_M)} dE,$$
 (1)

where A^* is the modified Richardson constant, T is the temperature, k is Boltzmann constant, T(E) is the energy-dependent transmission probability, $f_{\rm M}$ and $f_{\rm S}$ are the Maxwellian distribution functions at the metal contact and in the SSO, respectively, and $E_{\rm CS}$ is the minimum conduction band energy in the SSO. Nilsson's approximation was used to determine the Fermi-level position in the degenerately doped SSO, 17 and image force barrier lowering was taken into account.

The value of T(E) was calculated using the Wentzel-Kramers-Brillouin (WKB) approximation:

$$T(E) = \exp\left(-2\int_0^{x_{max}} \kappa(E) \cdot dx\right), \text{ for } E < EC(x),$$
 (2)

where x is the distance into the SSO from the metal interface, $\kappa(E)$ is the wave number, and x_{max} is the end point for the tunneling integration. $\kappa(E)$ was calculated using

$$\kappa(E) = \frac{\sqrt{2m^*(E_C(x) - E)}}{\hbar},\tag{3}$$

where $E_C(x)-E$ is the energy below the conduction band edge, m^* is the electron effective mass, and \hbar is the reduced Planck's constant. A parabolic profile was assumed for $E_C(x)$. A dielectric constant, K_S , of 17.8 for SSO was used, ¹⁸ while m^* was assumed to be 0.35 m_0 . ¹⁰ Finally, ρ_C was calculated as the inverse derivative of J vs V at V=0, where V is the applied bias.

Figure 5 shows a plot of ρ_C vs T for SSO_Control, comparing the experimental results with our theoretical model. An optimization was performed to determine the values of the Schottky barrier height, Φ_{B} , and doping concentration, $N_{\rm D}$, that best fit the data. The optimization results show a doping concentration of $5.8 \times 10^{19} \, \text{cm}^{-3}$ and a barrier height, Φ_B , of 0.76 eV. The barrier height value indicates that some degree of Fermi-level pinning occurs at the Ti/SSO interface, since this value is higher than the 0.30 eV expected based upon a 4.3 eV work function for Ti and a 4.00 eV electron affinity for SSO. 19 However, this value is comparable with Φ_B values obtained for Ti and TiS₂ contacts on Si.²⁰ The extracted doping concentration of $5.8 \times 10^{19} \, \text{cm}^{-3}$ in the model was necessary to account for the weak temperaturedependence, which cannot be explained with lower doping levels. (Figure S4 shows simulation results for values of N_D and Φ_B .) This result suggests that the carrier concentration beneath the contacts increases, possibly due to oxygen vacancy formation after annealing, though additional studies are needed to fully understand this behavior.

The smallest $\rho_{\rm C}$ values reported here for SSO are still higher by ~ 1 order of magnitude (~ 3 orders of magnitude) than those reported on GaN²¹ for a doping of $6 \times 10^{17} \, {\rm cm}^{-3}$ ($10^{20} \, {\rm cm}^{-3}$), suggesting that further optimization is needed to be competitive with this more mature semiconductor technology. The $\rho_{\rm C}$ value of $0.001 \pm 0.002 \, {\rm m}\Omega{\rm -cm}^2$ obtained on the SSO_Bilayer film, despite the large error bar,

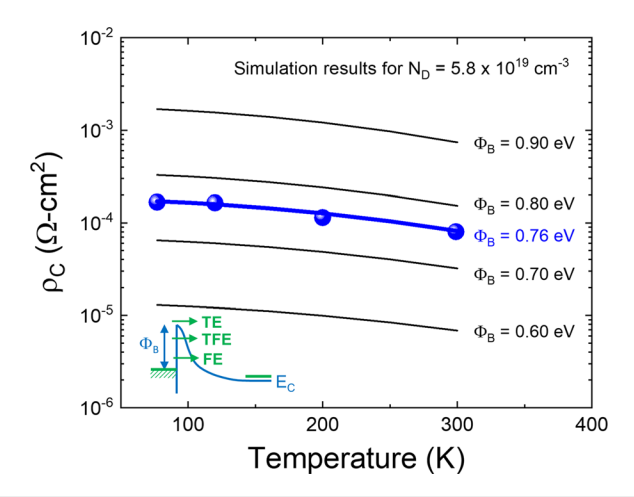


FIG. 5. Plot of specific contact resistivity, $\rho_{\rm C}$, vs temperature for experimental Ticontacts to SSO_Control after 300 °C annealing (blue points) and simulated contacts for 5.8 × 10¹⁹ cm⁻³ doped SSO with Schottky barrier height, $\Phi_{\rm B}$, of 0.76 eV (blue line). The simulated $\rho_{\rm C}$ values between 0.6 eV and 0.9 eV are also shown (black lines). Inset: diagram of Schottky barrier injection model used for theoretical calculations showing field emission (FE), thermionic field emission (TFE), and thermionic emission (TE) mechanisms. The weak temperature dependence indicates that FE is the dominant transport mechanism.

has a worst-case value of 3 $\mu\Omega$ -cm², which is within the same order of magnitude as those reported on β -Ga₂O₃²² at a doping of 5×10^{19} cm⁻³. Lower E_G intermediate layers, such as indium tin oxide (ITO), have also been deposited on emerging UWG semiconductors, such as β -Ga₂O₃²³ and AlGaN²⁴ via sputtering to achieve similar ρ_C values to those reported on SSO in this work. A similar approach may also be used for SSO by growing an epitaxial (or sputtered) BaSnO₃ on top of SSO in order to exploit the higher achievable doping and conductivity in BaSnO₃ to further reduce R_C and ρ_C . ^{25,26}

In conclusion, we have performed an analysis of metal contact resistance to Nd-doped SrSnO₃ thin films grown by MBE. Ti contacts were found to provide the best overall performance with Ohmic behavior and low variability. Contact resistance and specific contact resistivity values as low as $2.4 \pm 0.3 \ \Omega$ -mm and $0.03 \ \text{m}\Omega$ -cm², after ALD Al₂O₃ passivation at 200 °C, were extracted for Ti contacts to SSO with $2.3 \times 10^{19} \, \text{cm}^{-3}$ donor density. Subsequent annealing at 300 °C did not result in any significant change in the contact resistance. Temperature-dependent analysis of Ti contacts to lighter-doped device samples indicates that the contact resistance is dominated by field emission. The heavily doped bi-layer device samples have sufficiently low contact resistance to be within the error of the measurement, but the worst-case values are comparable with other UWG semiconductors. This work is an important step for evaluating SrSnO₃ for electronic device applications, including high-performance and transparent electronics, and may help attain lower contact resistances.

See the supplementary material for detailed process flow, TLM results before annealing, contact resistance summary tables, and additional data on theoretical model fitting results.

This work was primarily supported by the AFOSR through Award No. FA9550-19-1-0245. This work was supported partially by the National Science Foundation (NSF) through No. DMR-1741801 and the University of Minnesota MRSEC under Award No. DMR-2011401. Portions of this work were carried out in the Characterization Facility, University of Minnesota, which receives partial support from the NSF through the MRSEC under Award No. DMR-2011401 and the Minnesota Nano Center, which receives support from the NSF through the National Nanotechnology Coordinated Infrastructure (NNCI) under Award No. ECCS-2025124.

DATA AVAILABILITY

The data that support the findings of this study are available from the corresponding author upon reasonable request.

REFERENCES

¹J. Y. Tsao, S. Chowdhury, M. A. Hollis, D. Jena, N. M. Johnson, K. A. Jones, R. J. Kaplar, S. Rajan, C. G. V. D. Walle, E. Bellotti, C. L. Chua, R. Collazo, M. E. Coltrin, J. A. Cooper, K. R. Evans, S. Graham, T. A. Grotjohn, E. R. Heller, M. Higashiwaki, M. S. Islam, P. W. Juodawlkis, M. A. Khan, A. D. Koehler, J. H. Leach, U. K. Mishra, R. J. Nemanich, R. C. N. Pilawa-Podgurski, J. B. Shealy, Z. Sitar, M. J. Tadjer, A. F. Witulski, M. Wraback, and J. A. Simmons, "Ultrawide-bandgap semiconductors: Research opportunities and challenges," Adv. Electron. Mater. 4, 1600501 (2018).

²W.-J. Lee, H. J. Kim, J. Kang, D. H. Jang, T. H. Kim, J. H. Lee, and K. H. Kim, "Transparent perovskite barium stannate with high electron mobility and thermal stability," Annu. Rev. Mater. Res. 47, 391 (2017).

³K. Krishnaswamy, B. Himmetoglu, Y. Kang, A. Janotti, and C. G. V. D. Walle, "First-principles analysis of electron transport in BaSnO₃," Phys. Rev. B **95**, 205202 (2017).

⁴A. B. Abd Rahman, M. S. Sarjadi, A. Alias, and M. A. Ibrahim, "Fabrication of stannate perovskite structure as optoelectronics material: An overview," J. Phys.: Conf. Ser. **1358**, 012043 (2019).

E. Baba, D. Kan, Y. Yamada, M. Haruta, H. Kurata, Y. Kanemitsu, and Y. Shimakawa, "Optical and transport properties of transparent conducting Ladoped SrSnO₃ thin film," J. Phys. D 48, 455106 (2015).
W. Zhang, J. Tang, and J. Ye, "Structural, photocatalytic, and photophysical

^oW. Zhang, J. Tang, and J. Ye, "Structural, photocatalytic, and photophysical properties of perovskite MSnO₃ (M = Ca, Sr., and Ba) photocatalysts," J. Mater. Res. **22**, 1859–1871 (2007).

M. Wei, A. V. Sanchela, B. Feng, Y. Ikuhara, H. J. Cho, and H. Ohta, "High electrical conducting deep-ultraviolet-transparent oxide semiconductor Ladoped SrSnO₃ exceeding ~3000 S cm⁻¹," Appl. Phys. Lett. 116, 022103 (2020).
A. Prakash, N. F. Quackenbush, H. Yun, J. Held, T. Wang, T. Truttmann, J. M. Ablett, C. Weiland, T.-L. Lee, J. C. Woicik, K. A. Mkhoyan, and B. Jalan, "Separating electrons and donors in BaSnO₃ via band engineering," Nano Lett. 19, 8920–8927 (2019).

⁹T. Wang, L. R. Thoutam, A. Prakash, W. Nunn, G. Haugstad, and B. Jalan, "Defect-driven localization crossovers in MBE-grown La-doped SnSnO₃ films," Phys. Rev. Mat. 1, 061601 (2017).

¹⁰T. Wang, A. Prakash, Y. Dong, T. Truttmann, A. Bucsek, R. James, D. D. Fong, J.-W. Kim, P. J. Ryan, H. Zhou, T. Birol, and B. Jalan, "Engineering SrSnO₃ phases and electron mobility at room temperature using epitaxial strain," ACS Appl. Mater. Interfaces 10, 43802–43808 (2018).

¹¹T. Truttmann, A. Prakash, J. Yue, T. E. Mates, and B. Jalan, "Dopant solubility and charge compensation in La-doped SrSnO₃ films," Appl. Phys. Lett. 115, 152103 (2019).

¹²V. R. S. K. Chaganti, A. Prakash, J. Yue, B. Jalan, and S. J. Koester, "Demonstration of a depletion-mode SrSnO₃ n-channel MESFET," IEEE Elect. Dev. Lett. 39, 1381–1384 (2018).

¹³V. R. S. K. Chaganti, T. K. Truttmann, F. Liu, B. Jalan, and S. J. Koester, "SrSnO₃ field-effect transistors with recessed gate electrodes," IEEE Elect. Dev. Lett. 41, 1429–1431 (2020).

¹⁴J. Wen, V. R. S. K. Chaganti, T. K. Truttmann, F. Liu, B. Jalan, and S. J. Koester, "SrSnO₃ metal-semiconductor field-effect transistor with GHz operation," IEEE Elect. Dev. Lett. 42, 74–77 (2021).

¹⁵A. Prakash, P. Xu, X. Wu, G. Haugstad, X. Wang, and B. Jalan, "Adsorption-controlled growth and the influence of stoichiometry on electronic transport in

- hybrid molecular beam epitaxy-grown BaSnO3 films," J. Mater. Chem. C 5, 5730–5736 (2017).
- 16E. L. Murphy and R. H. Good, "Thermionic emission, field emission and the transition region," Phys. Rev. 102, 1464–1472 (1956).
- ¹⁷N. G. Nilsson, "Empirical approximations for the Fermi energy in a semiconductor with parabolic bands," Appl. Phys. Lett. 33, 653–654 (1978).
- ¹⁸I. Petousis, D. Mrdjenovich, E. Ballouz, M. Liu, D. Winston, W. Chen, T. Graf, T. D. Schladt, K. A. Persson, and F. B. Prinz, "High-throughput screening of inorganic compounds for the discovery of novel dielectric and optical materials," Sci. Data 4, 160134 (2017).
- ¹⁹L. Bjaalie, B. Himmetoglu, L. Weston, A. Janotti, and C. G. Van de Walle, "Oxide interfaces for novel electronic applications," New J. Phys. 16, 025005 (2014).
- ²⁰M. O. Aboelfotoh and K. N. Tu, "Schottky-barrier heights of Ti and TiSi₂ on n-type and p-type Si(100)," Phys. Rev. B 34, 2311–2318 (1986).
- ²¹C. Lu, H. Chen, X. Lv, X. Xie, and S. N. Mohammad, "Temperature and doping-dependent resistivity of Ti/Au/Pd/Au multilayer Ohmic contact to n-GaN," J. Appl. Phys. 91, 9218–9224 (2002).

- ²²K. Sasaki, M. Higashiwaki, A. Kuramata, T. Masui, and S. Yamakoshi, "Si-ion implantation doping in β -Ga₂O₃ and its application to fabrication of low-resistance Ohmic contacts," Appl. Phys. Express **6**, 086502 (2013).
- ²³P. H. Carey, J. Yang, F. Ren, D. C. Hays, S. J. Pearton, A. Kuramata, and I. I. Kravchenko, "Improvement of Ohmic contacts on Ga₂O₃ through use of ITO-interlayers," J. Vac. Sci. Technol. B 35, 061201 (2017).
- ²⁴H. Wang, Q. Zhou, S. Liang, and R. Wen, "Fabrication and characterization of AlGaN-based UV LEDs with a ITO/Ga₂O₃/Ag/Ga₂O₃ transparent conductive electrode," Nanomaterials 9, 66 (2019).
- 25A. Prakash, P. Xu, A. Faghaninia, S. Shukla, J. W. Ager, C. S. Lo, and B. Jalan, "Wide bandgap BaSnO₃ films with room temperature conductivity exceeding 10⁴ S cm⁻¹," Nat. Commun. 8, 15167 (2017).
- ²⁶H. Paik, Z. Chen, E. Lochocki, A. Seidner H., A. Verma, N. Tanen, J. Park, M. Uchida, S. Shang, B.-C. Zhou, M. Brützam, R. Uecker, Z.-K. Liu, D. Jena, K. M. Shen, D. A. Muller, and D. G. Schlom, "Adsorption-controlled growth of La-doped BaSnO₃ by molecular-beam epitaxy," APL Mater. 5, 116107 (2017).